Indian Geotech J
https://doi.org/10.1007/s40098-024-00940-7

ORIGINAL PAPER

# Investigation on Load Transfer in Geosynthetic-Reinforced Pile-Supported Embankments

**Muhan Yan**[1,2,3] · **Shuaijie Guo**[2,3] · **Haiyang Zhang**[2,3] · **Xuguo Song**[2,3] · **Hong Xiao**[1]

Received: 13 June 2023 / Accepted: 14 March 2024


**Abstract** The geosynthetic-reinforced pile-supported embankment (GRPSE) is one of the most effective and economical foundation reinforcement measures for embankment constructed over soft soils. The 3D analysis using finite element method was adopted to study the soil arching effect of GRPSEs, including load transfer between piles and soils. In this study, the numerical model has been calibrated with measured data obtained from field tests conducted along the alignment of a high-speed railway in China. The results of subsequent parametric study show significant correlations between pile efficiency and the height of the embankment, the pile spacing, the tensile strength of the geogrid, and slope of the virgin consolidation curve of the soil. Models used in previous studies have not fully represented the effects of the properties of geogrids and soils on the soil arching effect. An empirical calculation model that considers the four factors mentioned and based on multi-shell arching theory was presented. This model can be used to calculate the vertical stresses in the embankment, especially in the cushion, and the pile efficiency.

**Keywords** Geosynthetics · Piled embankments · Finite element analysis · Load transfer · Soil arching · Empirical method

✉ Muhan Yan
ymh_hit@163.com

1 School of Civil Engineering of Beijing Jiaotong University, Beijing, China

2 China Railway Design Corporation, Tianjin, China

3 National Engineering Research Center for Digital Construction and Evaluation of Urban Rail Transit, Tianjin, China

## Introduction

When designing structures over soft soils, geotechnical engineers face several challenges because of the poor engineering properties of such soils, such as their high compressibility, low bearing capacity, low permeability, and high moisture content. High-speed railways require high-quality embankments, and soft soil foundations lead to severe problems, such as bearing capacity failure, excessive total and differential settlements, lateral flow of soil, and global instability [1, 2]. GRPSE system provides an economic and effective solution to these problems, because of its short construction time and low maintenance charge [3, 4]. The inserted geosynthetic layers work together with the embankment and piles to enhance the load transfer efficiency, minimize the yielding deformation of subgrade fill above piles, and feasibly reduce the total and differential settlements of embankment [5, 6].

The design of GRPSEs includes the geometric design of embankment, the layout of piles and geosynthetic reinforcement, and the determination of appropriate construction material properties. The existing design methods for GRPSEs, such as BS8006, EBGEO, CUR226, and FHWA [7, 8], adopt the concept of various theories of soil arching [9–12]. The methods mentioned above were developed for individual countries and suitable for that specific geological and national conditions. These design methods also followed diverse conservative hypotheses and simplification. Current design methods exhibited great differences in their load transfer predictions and leaded to very different results [13–16], which was indicated by Filz and Smith [17] and Nunez et al. [18]. However, there is no any design method for GRPSEs in any countries, including China. Thus, this study focused on a method to calculate the load transfer applicable to China's high-speed railway.

There are three categories of analytical methods widely accepted to estimate the load distribution inside a granular cushion. The first category is that of empirical methods, which are derived from the equilibrium of the volume of soil during redistribution with loads transferring along the shearing surface at the edge of pile [8]. The second category is that of methods assuming load transfer is due to the dead weight of a stable soil wedge above the piles [19, 20]. The third category is to establish equilibrium equations of the arches between adjacent piles [8, 11, 21]. Differences among different types of methods may be owing to the fact that they are based on the results of small-scale models or numerical analyses, as opposed to in situ conditions. Another possible reason for the differences among different types of methods is that most of the theoretical models assume that the soil arching is at a fully mobilized or limit equilibrium state. However, only partially mobilized arching is developed in practice, which may change the load transmission and pile efficiency [22].

Because load transfer in GRPSEs is a complex phenomenon depends on a number of factors, numerical techniques are needed to analyse the responses of such embankments accurately [23, 24]. To study the stress redistribution from soil to piles, the tensile forces, and the strains of geosynthetic in the cushion layer, three-dimensional (3-D) analyses are required [16, 17, 25].

The reliability of some soil arching theories has been studied based on the field tests results of a China's high-speed railway. Through this study, an empirical method has been presented with borrowed multi-shell arching theory to predict the load transfer in a GRPSE appropriate for GRPSEs in China.

## Section Conditions

In this study, a GRPSE section of Wuhan–Guangzhou high-speed railway in China was selected as the base case for the numerical modelling, which is shown in Fig. 1. The profile of the soil is as follows: there is about 4.5 to 10.7 m thick of soft soil overlying a 3.5 to 6.1 m thick deposit of cobbly soil that overlies approximately 8.9 to 10.9 m thick of silty clay. The bearing stratum below is limestone. The foundation is reinforced by CFG piles with a diameter of 0.5 m and centre-to-centre spacing of 2.5 m. The top 0.3 m of the piles are square pile heads with a side length of 1.5 m. Two layers of biaxial polypropylene grid are sandwiched between 0.6-m-thick gravel layers at a spacing of 0.3 m. The embankment was designed with a full height of 6.0 m. Out of this total height, 4.7 m was constructed over a period of 5 months and subsequently rested for 3 months. Vertical pressures in the embankment were measured at 0.3 m above the ground level (just between two layers of geogrids) by 4 earth pressure cells with a precision of 1% F.S. and a maximum range of 0.4 MPa. The horizontal layout of 4 earth pressure cells is shown in Fig. 2a, P1, P2 above the pile cap and S1, S2 above the soil. The settlement at the ground level beside point S1 was also monitored by a settlement gauge with a precision

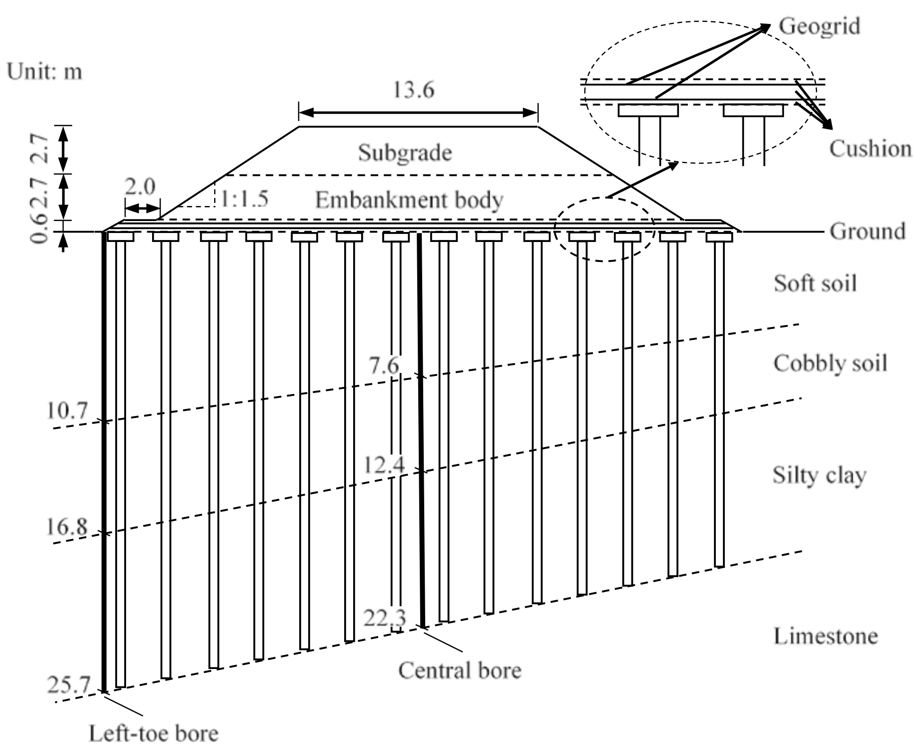


**Fig. 1** Typical cross section of geogrid-reinforced pile-supported embankment

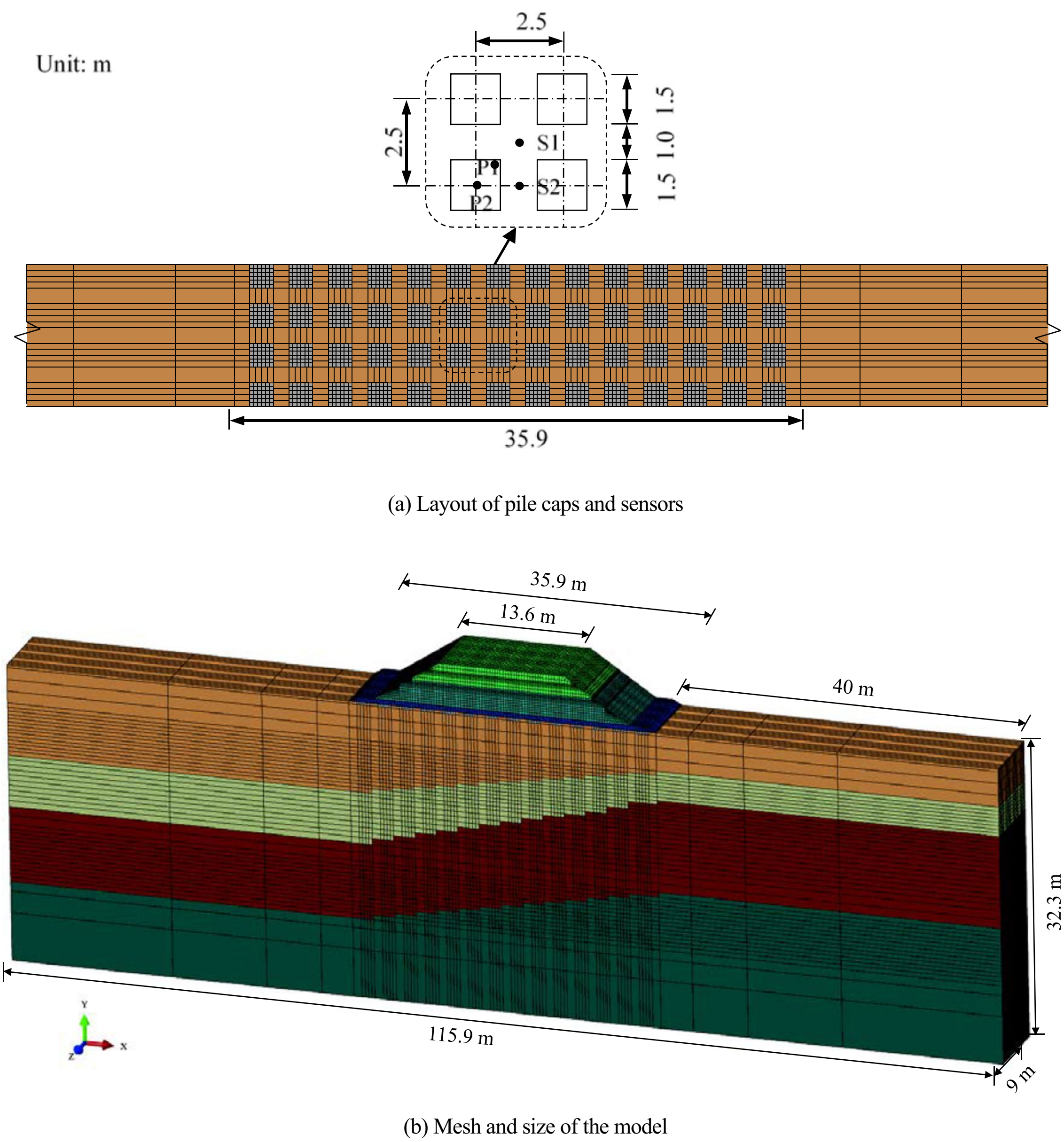


**Fig. 2** Finite element models adopted in the numerical analyses

of 0.1 mm and a maximum range of 100 mm. More details were reported by Cai et al. [26].

## Finite Element Modelling

A three-dimensional finite element model was established to simulate the GRPSE system using finite element modelling software named ABAQUS. The soil layers were modelled using eight-node brick elements with reduced integration coupled pore pressure (C3D8RP). C stands for continuum stress/displacement, 3D for three-dimensional, 8 for eight nodes, R for reduced integration, and P for pore pressure. This type of element has good stress and strain resolving ability with good convergence. Fully drained conditions were assumed for the cushion, embankment body, and the subgrade, because of the relatively high permeability of these parts in comparison with others, which is why they were modelled using eight-node brick elements with reduced integration but without considering pore pressure (C3D8R). The geogrid was modelled using three-dimensional four-node membrane elements with reduced integration (M3D4R). This type of element transmits only surface forces (no moments) and has no bending stiffness [27].

Figure 2b shows the details of numerical model conducted in this investigation. The foundation was considered to be 18.9- to 25.7-m-thick layer overlying a rigid impermeable stratum. To minimize the boundary effects, the horizontal length of the model was taken to be 115.9 m in the $x$-direction, which was more than 3 times the width of the embankment base [28]. Four rows of piles were arranged in the $z$-direction of embankment of 9 m. The transverse and lateral behaviour of the embankment was evaluated systematically by the middle two rows of piles in 5-m-wide section. The bottom was assumed to be fixed boundary, which means displacements in all three directions were set to 0. The horizontal boundaries (in the $x$-direction) and along the track (in the $z$-direction) were set to be smooth and rigid (zero displacements in these two directions, respectively). All these boundaries were defined to be impermeable [29].

The zero-pore-pressure boundary was established so that pore fluid could flow only through the top surface of the ground [30]. The end of the geogrid was fixed laterally at the toe and at the cross section of the embankment but was allowed to move freely in the vertical direction with the cushion.

The interaction between the geogrid and the cushion was stimulated by using the surface-to-surface contact. The normal interface contact was defined to be 'hard contact' and not allowed to be separated [31]. Furthermore, the interaction of shear resistance was simulated using the Coulomb friction in the tangential direction. The geogrid–cushion interface friction angle was assumed to be equal to the friction angle of the cushion. The pile behaviour was affected by the interaction of soil–pile interface. A Coulomb frictional model, with a friction coefficient of 0.3, was also used to model the frictional behaviour [32].

For simplicity, the subgrade, the embankment body, the cushion, the cobbly soil, and the silty clay were modelled using Mohr–Coulomb failure criteria. Given the high stiffness and small deformation of the piles and limestone, these two components were simulated as linearly elastic materials. However, because the behaviour of the soft soil layer obviously affects the GRPSE, the modified Cam–Clay model was applied to simulate the significant plastic deformation. This model explains the elastic–plastic deformation characteristics of normal consolidated clay well, especially considering the plastic volume deformation. All model parameters can be obtained by triaxial tests. The material property values used in the baseline case are listed in Tables 1 and 2, which were obtained by a series of field and laboratory tests.

Construction of an embankment over soft soil is often performed in stages to ensure the embankment's stability and minimize the post-construction settlement. The total construction time was about 8 months as shown in Fig. 3. Each stage has construction process and waiting process, and the excess pore water pressure dissipates partially in waiting process. However, because of the difficulty the actual staged construction process was simplified as the grey line in Fig. 3. The whole embankment was 6.0 m high, but field tests were completed when the embankment reached 4.7 m high. Therefore, although the full model represents a 6.0-m-high embankment, the simulation ended when the embankment reached 4.7 m.

## Validation of the Embankment Model

The settlement distribution of the foundation 93 days after construction is shown in Fig. 4. The maximum settlement

**Table 1** Material parameter values for FEM analysis (1)

| Material | Density, $\rho$ (kg/m$^3$) | Elastic modulus, $E$ (MPa) | Friction angle, $\varphi$ (°) | Cohesion, $c$ (kPa) | Poisson's ratio, $\upsilon$ | Initial void ratio, $e$ | Permeability coefficient, $k_w$ (m/day) |
|---|---|---|---|---|---|---|---|
| Subgrade | 2200 | 60 | 38 | 3 | 0.3 | – | – |
| Embankment body | 1950 | 37 | 31 | 7 | 0.3 | – | – |
| Cushion | 1780 | 50 | 44 | 1 | 0.3 | – | – |
| Cobbly soil | 2300 | 44 | 24 | 13 | 0.3 | 0.68 | $3.04\times10^{-3}$ |
| Silty clay | 1950 | 46 | 22 | 28 | 0.35 | 0.86 | $1.18\times10^{-3}$ |
| Limestone | 2700 | 25,000 | – | – | 0.2 | – | – |
| Geogrid | 40 | 640 | – | – | 0.2 | – | – |
| Pile | 2400 | 28,000 | – | – | 0.167 | – | – |

**Table 2** Material parameter values for FEM analysis (2)

| Material | Density, $\rho$ (kg/m$^3$) | Poisson's ratio, $\upsilon$ | $\lambda$ | $\kappa$ | $M$ | Void ratio, $e_1$ | Permeability coefficient, $k_w$ (m/day) |
|---|---|---|---|---|---|---|---|
| Soft soil | 1700 | 0.35 | 0.2 | 0.04 | 1.05 | 1.2 | $6.51\times10^{-4}$ |

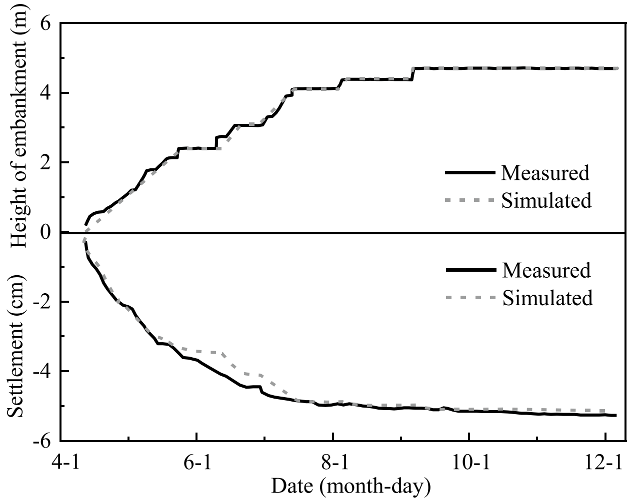


**Fig. 3** Comparison between measured and calculated settlement of ground during construction

of foundation occurs between the central rows of piles. Figure 5 shows the vertical stress distribution of embankment 93 days after construction. The stress concentration at the piles and the soil arching in the embankment are apparent in Fig. 5a. The stress concentration phenomenon occurs on the pile head, and the subsoil body around the pile head forms an arching shape. The maximum vertical stress occurs above the corner of pile caps, as shown in Fig. 5b, which may due to the stress concentration at the edge of them. Figure 3 shows a comparison between the foundation soil settlement during the embankment construction period, as predicted by 3D FEM model, and the values measured during the field tests. There is a consistency in the settlements of the ground surface between FEM simulated and measured. The settlements measured during June and July were greater than those simulated. This is probably because the gravel is redistributed to produce soil arching and the cushion moves slowly into the soil between piles when the height of embankment is approximately 2.5 m. Figure 6 shows a comparison between the vertical stress 0.3 m above the ground, as predicted by the numerical model, and the vertical stresses measured in the field tests during construction. This comparison shows that the FEM could accurately simulate the vertical stress.

As the real stratum is tilted and is not universal, a GRPSE on horizontal stratum was simulated then as

**Fig. 4** Settlement distribution of the foundation 93 days after construction (m)

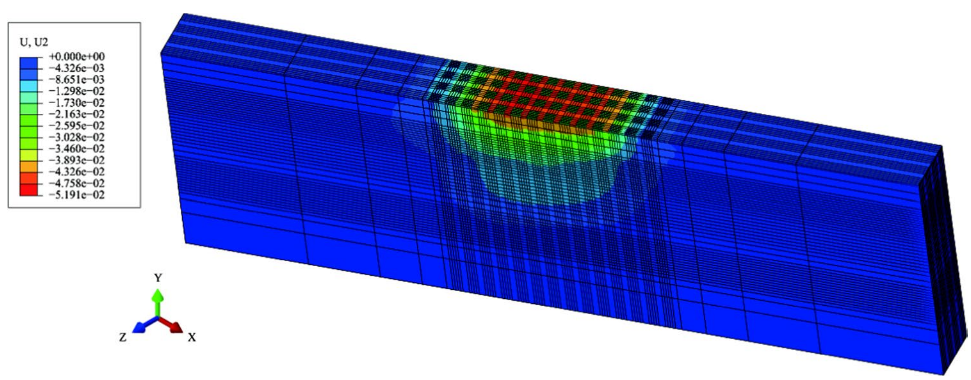


**Fig. 5** Vertical stress distribution of embankment 93 days after construction (kPa)

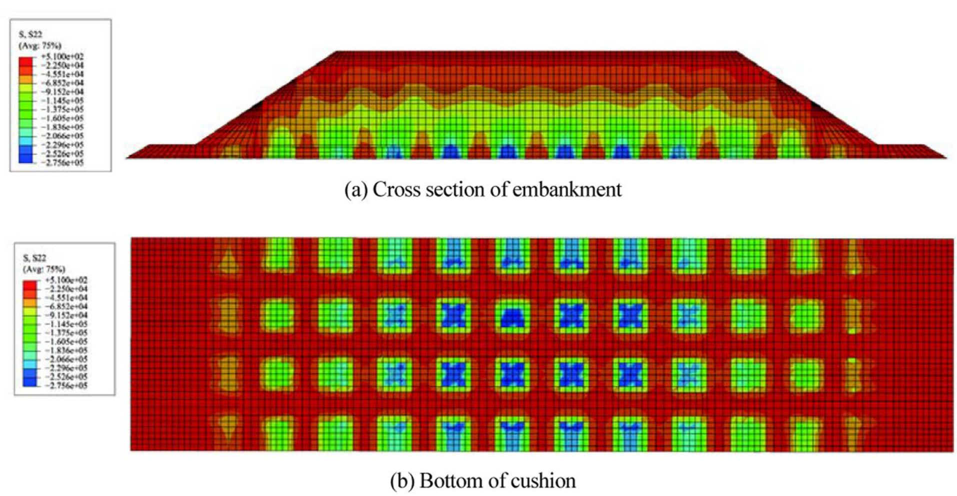

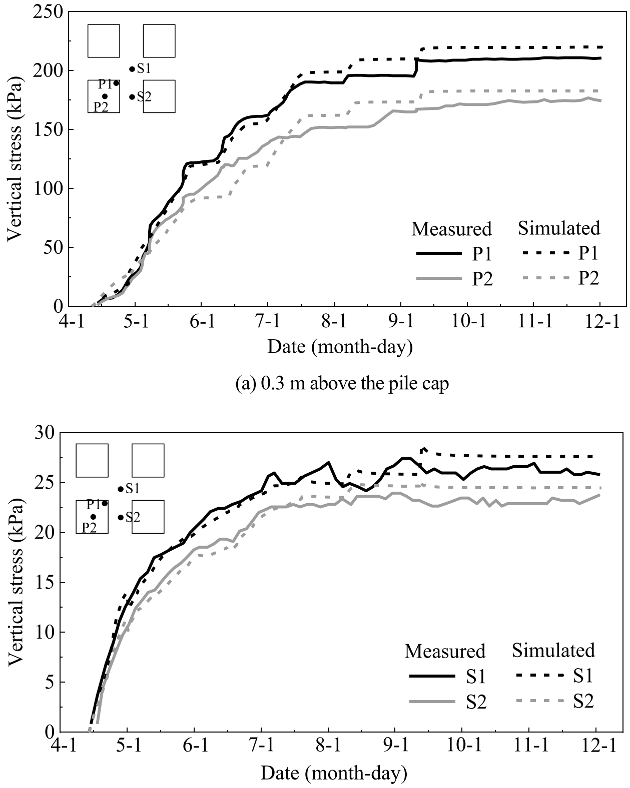


(a) 0.3 m above the pile cap

(b) 0.3 m above the surrounding soil

**Fig. 6** Distribution of vertical stress

shown in Fig. 7a. The properties of materials and the sizes of embankments were the same. The tilted stratum was adjusted to be horizontal, and the thickness of three layers was 7.6, 4.8, and 9.9 m, respectively, which was the average thickness of real stratum. The layout of geogrids and piles was the same and every pile dug down to the limestone layer. The settlement and vertical stress cloud charts of these two models were similar and were not listed in the paper. The landmark indexes of these two models are shown in Fig. 7b. It is indicated by comparison that the adjustment of stratum is reasonable. The settlement and vertical stress of adjusted model were slightly smaller than origin model that's because the observation points were at the side of thicker soft soil. The subsequent analyses were therefore based on the horizontal stratum model.

## Vertical Stress Distribution in the Embankment

The distribution of vertical stress in the embankment on horizontal stratum is shown in Fig. 8a. It has been seen that the vertical stress initially increases with depth and then changes at a height of approximately 2.5 m above the ground. The vertical stress above the soil decreases with increasing vertical stress above the pile cap. Further differences are evident below a height of 0.6 m, which is just within the range of geogrid and cushion. The soil inside a soil arch should fall under the influence of gravity. However, the geogrid supports the soil and transmits the load to the arch springing, and less vertical stress needs to be supported by the soft soil of the foundation. These phenomena illustrate the redistribution of vertical stresses caused by soil arching and the tensioned membrane action of the cushion with geogrid.

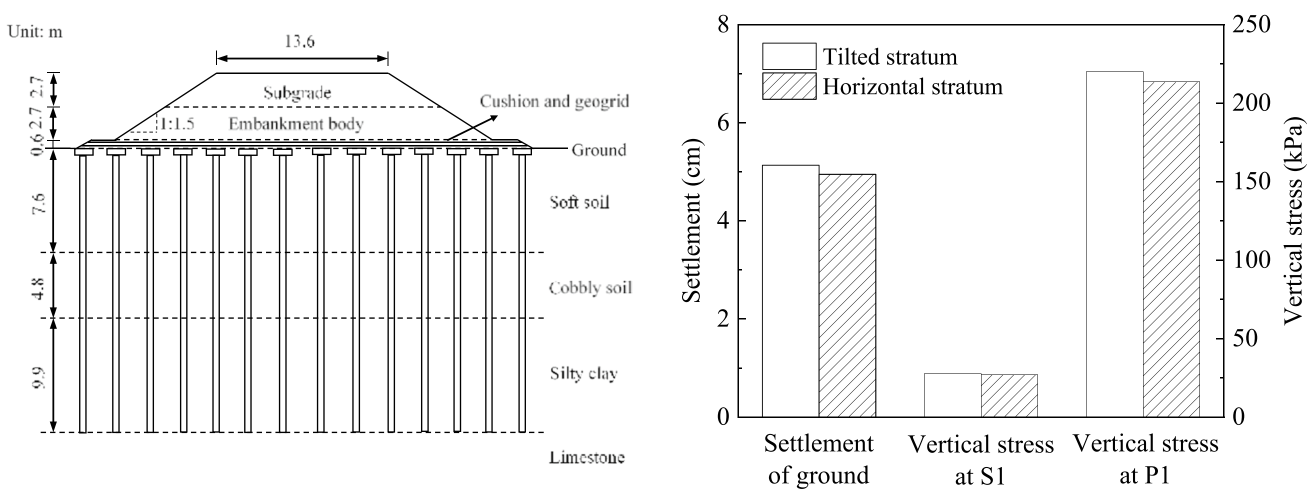


(a) Cross section of GRPSE on horizontal stratum

(b) Comparison of simulated results in different stratum conditions

**Fig. 7** Condition of GRPSE on horizontal stratum

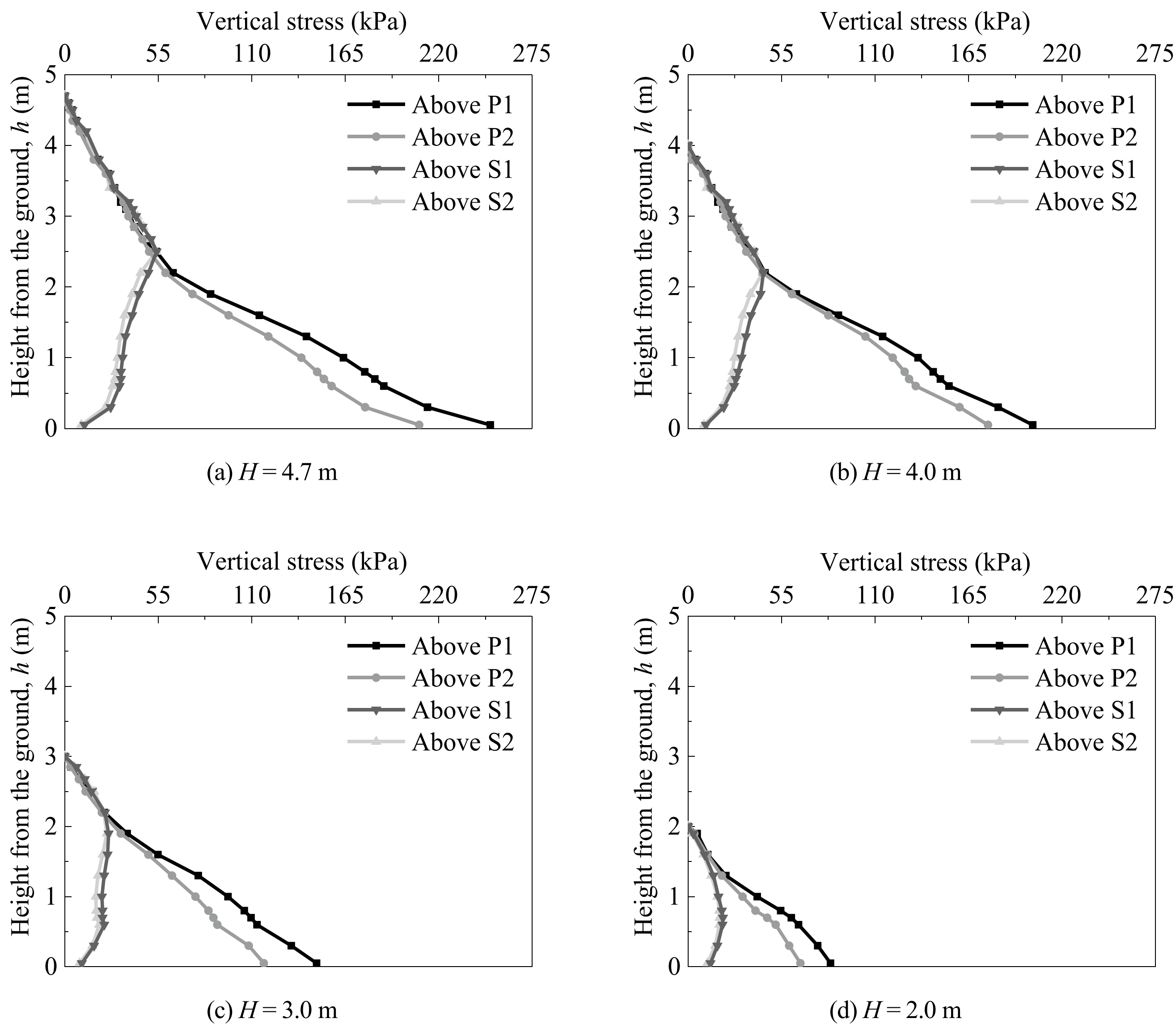


**Fig. 8** Influence of embankment height ($H$) on the distribution of vertical stress ($s = 2.5$ m)

## Parametric Study

As the slope of the high-speed railway embankment is fixed and the selection of the filler is clearly defined, in this study, the following four key influence factors were considered to investigate the behaviour of the GRPSEs: (1) the embankment height ($H$), with values of 4.7, 4, 3, and 2 m; (2) the pile spacing ($s$), with values of 3.0, 2.5, 2.0, and 1.8 m; (3) the tensile strength of the geogrid ($J$), with values of 20, 40, 80, 100, and 200 kN/m; and (4) slope of the virgin consolidation curve of the soil ($\lambda$), with values of 0.05, 0.1, 0.15, 0.2, and 0.25. For each case, only one parameter was varied. Fifteen cases were investigated.

The distributions of vertical stress with respect to embankment height are shown in Fig. 8. It has been seen that the distributions of vertical stress are similar when $H = 4.7$, 4.0, and 3.0 m. In these conditions, the height of soil arching slightly decreases with the embankment height. The vertical stress above the pile cap apparently increases with the embankment height, while the vertical stress above the soil is almost unchanged. This difference shows the redistribution of the vertical stresses caused by the soil arching and most of the load transfer to the pile. However, soil arching is not clearly evident in Fig. 8d. This is probably because the embankment height is not sufficient to form a soil arching. The vertical stress above piles is still greater than that above soil because of the stress concentration effect rather than the soil arching effect.

Figure 9 shows the distributions of vertical stress for different pile spacing. It has been seen that the distributions of

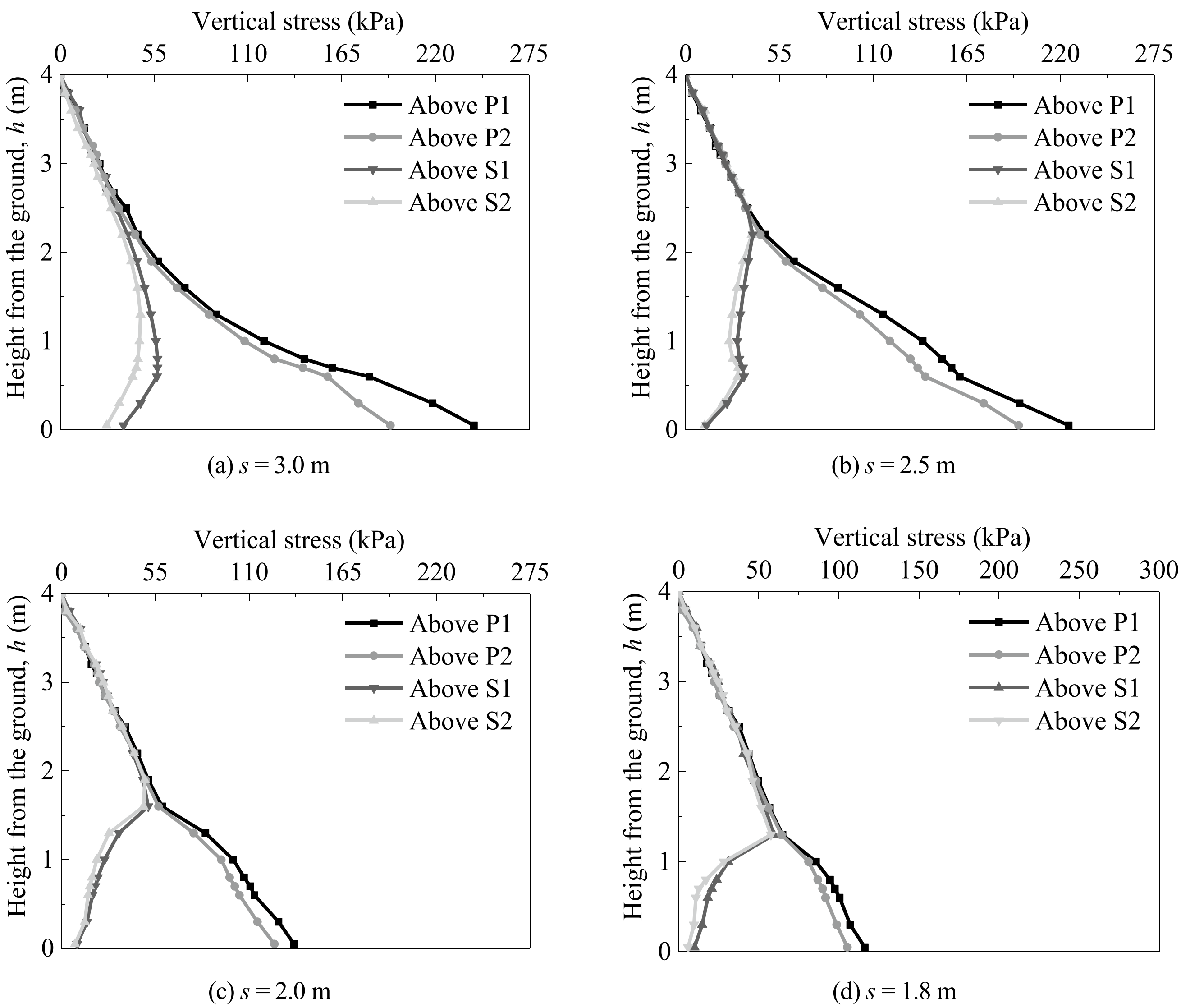


**Fig. 9** Influence of pile spacing ($s$) on the distribution of vertical stress ($H=4.0$ m)

vertical stress are similar when $s=2.5$, 2.0, and 1.8 m. Under these conditions, the height of soil arching decreases significantly with the pile spacing. The vertical stress above the pile cap apparently decreases with the embankment height, while the vertical stress above the soil remains almost unchanged. This is because, although the embankment fill above soil arching becomes thicker with lower soil arching, the dead load above soil arching decreases with less spacing between adjacent piles. However, soil arching is not clearly evident in Fig. 9a. This is probably because the pile spacing is too great and the shear strength of the embankment fill is not sufficiently great to form a complete soil arch of that size.

The effects of the tensile strength of the geogrid and slope of the virgin consolidation curve of the soil were also studied. The trend of vertical stress distribution curve is the same as that in other cases, so these two effects are discussed in another way in the following sections.

## A Modified Empirical Model Based on Multi-Shell Arching Theory

The EBGEO (GGS 2010) method employs multi-shell arching theory to determine the stress distribution appearing on the pile and surrounding soil. The method is based on the conceptual 3-D soil arching conceptual presented by Hewlett [11], modified on the basis of a series of findings from theoretical analysis, experimental research, and engineering practice. The theory is based on the principle of plastic mechanics and assumes that the orientation of the major principal stress is a certain function. The following equation is given to calculate the distribution of the vertical stress along the height of an embankment as a function of the friction angle, the height of the embankment, the pile spacing, and the pile diameter [21].

$$\sigma_z(z) = \left(\lambda_1 + h_g^2 \cdot \lambda_2\right)^{-\chi} \cdot \left(\lambda_1 + z^2 \cdot \lambda_2\right)^{\chi} \cdot \left\{ \left(H - h_g\right) \cdot \gamma + \frac{\left(h_g - z\right) \cdot \gamma \cdot \left(\lambda_1 + h_g^2 \cdot \lambda_2\right)^{\chi} \cdot \left(\lambda_1 + \frac{h_g^2 \cdot \lambda_2}{4}\right)^{-\chi} \cdot \left(4s \cdot \lambda_1 + h_g \cdot \left(-2d \cdot \left(K_{\text{krit}} - 1\right) \cdot z\right) + s \cdot h_g \cdot \lambda_2\right)}{s \cdot \left(4 \cdot \lambda_1 + h_g^2 \cdot \lambda_2\right)} \right\} \quad (1)$$

where $h_g = \begin{cases} s/2 & \text{for } H \geq s/2 \text{ (full arching)} \\ H & \text{for } H < s/2 \text{ (partial arching)} \end{cases}$, $K_{\text{krit}} = \tan^2\left(45^{\circ} + \frac{\varphi}{2}\right)$, $\chi = \frac{d \cdot (K_{\text{krit}} - 1)}{\lambda_2 \cdot s}$, $\lambda_1 = \frac{1}{8} \cdot (s - d)^2$, $\lambda_2 = \frac{s^2 + 2 \cdot d \cdot s - d^2}{2 \cdot s^2}$, $h_g$ is the height of soil arching, $s$ is the pile spacing, $d$ is the size of the pile cap, $H$ is the height of the embankment, $\gamma$ and $\varphi$ are the gravity and friction angle of the embankment fill, respectively.

The comparison between the simulated and calculated vertical stress distributions in the embankment is shown in Fig. 10a. It has been seen that the simulated and calculated vertical stresses at ground level and above the soil arching are approximate, but that there is a significant difference in the range of soil arching. This is probably because the effects of a geogrid and the foundation soil are not considered in Eq. (1). However, it cannot be denied that Zaeske presented a reasonable method based on the principle of plastic mechanics because it is soil that constitutes the arch. The proof therein is that if the calculated curve was moved from place A to place B, it has been seen that the shape of the curve of the calculated vertical stress (the red line) is quite similar to that of the curve of the simulated vertical stress (grey line and black line). This means that the multi-shell arching theory can be used to estimate the vertical stress on the cushion. Furthermore, a modified method was presented to estimate the vertical stress in the cushion. The vertical stresses at different positions are indicated from $\sigma_1$ to $\sigma_8$ as shown in Fig. 10b. A correction factor $\beta$ is introduced to calculate the vertical stress above the soil on the upper surface of the cushion. A factor $\eta$ for the stress transfer rate of the cushion was introduced to calculate the stress change

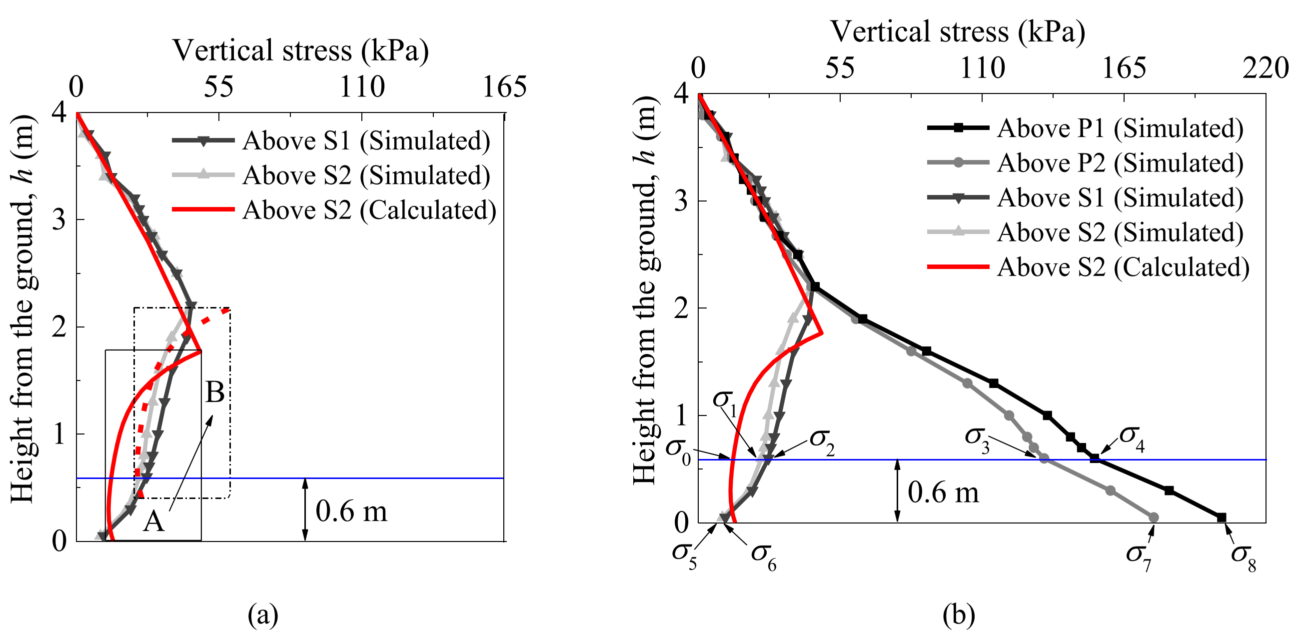


**Fig. 10** Comparison of simulated vertical stress in subgrade and that calculated via multi-shell arching theory (Color figure online)

from the upper surface of the cushion to the lower surface of the cushion. These factors are defined as follows:

$$\beta = \frac{\sigma_1}{\sigma_0} \tag{2}$$

$$\eta_{s1} = \frac{\sigma_2 - \sigma_6}{\sigma_2} \tag{3}$$

$$\eta_{s2} = \frac{\sigma_1 - \sigma_5}{\sigma_1} \tag{4}$$

$$\eta_{p1} = \frac{\sigma_8 - \sigma_4}{\sigma_4} \tag{5}$$

$$\eta_{p2} = \frac{\sigma_7 - \sigma_3}{\sigma_3} \tag{6}$$

in which $\sigma_0$ is the vertical stress above the soil, calculated using Eq. (1), $\sigma_1$ is considered to be equal to $\sigma_2$, $\sigma_5$ is considered to be equal to $\sigma_6$ and $\eta$ is the stress transfer rate of cushion above different points. $\beta$ and $\eta$ are related to the material properties and the size of the GRPSE system.

Finally, the vertical stress $\sigma_1$ above the soil on the upper surface of the cushion, the vertical stress $\sigma_5$ above the soil on the lower surface of the cushion, and the pile efficiency $E_p$ can be calculated from Eqs. (2, 7, and 8), respectively, which are very useful in engineering design.

$$\sigma_5 = \left(1 - \eta_{s2}\right) \cdot \beta \cdot \sigma_0 \tag{7}$$

$$E_p = \frac{F_p}{F} = 1 - \frac{F_s}{F} = 1 - \frac{\sigma_5 \cdot A_s}{\rho g H \cdot A} = 1 - \frac{\sigma_5 \cdot \left(s^2 - d^2\right)}{\rho g H \cdot s^2} \tag{8}$$

In these equations, $F$ is the total weight supported by the soil and piles, $F_s$ is the weight supported by the soil, $F_p$ is the weight supported by the pile caps, $A$ is the total area of the soil and pile caps, $A_s$ is the area of the soil, $\rho$ is the density of the embankment fill, and $g$ is the gravitational acceleration.

## Determination of Model Parameter Values

The only two parameters in the modified model whose values have to be determined are $\beta$ and $\eta$. As the quality of embankment fill has to conform to prevailing codes, its material properties must be consistent. The main influence factors are the height ratio of the embankment ($H'$), the area improvement ratio of the pile caps ($\alpha$), the tensile strength of the geogrid ($J$) and slope of the virgin consolidation curve of the soi ($\lambda$). The height ratio of the embankment is introduced to produce a dimensionless height parameter to make the analysis more reasonable.

$$H' = \frac{H}{d} \tag{9}$$

The dimensionless area improvement ratio is defined in the following manner to represent the influences of both the pile spacing and the size of the pile cap.

$$\alpha = 1 - \frac{A_s}{A} \tag{10}$$

Figure 11 shows the influences of the factors considered on $\beta$. Its value increases with $J$ but decreases with increasing $H'$ and $\lambda$. This is because the vertical stress calculated using Eq. (1) is a theoretical value that depends on the embankment fill and the pile cap. However, an increase in $J$ or a decrease in $H'$ or $\lambda$ weakens the soil arching or enhances the cushion, with the result that the cushion above the soil can support more load. The influence of $\alpha$ on $\beta$ is close to a quadratic function. It is apparent that the soil arching effect is maximized when the area improvement ratio is approximately 0.4. The simulated results can be well fitted by the following functions:

$$\beta_{H'} = -0.033 + 7.45/H' \quad R^2 = 0.979 \tag{11}$$

$$\beta_\alpha = 13.77 - 71.58\alpha + 132.13\alpha^2 - 73.54\alpha^3 \quad R^2 = 0.977 \tag{12}$$

$$\beta_J = 0.00234J + 1.6 \quad R^2 = 0.996 \tag{13}$$

$$\beta_\lambda = 1.321\lambda^{-0.202} \quad R^2 = 0.993 \tag{14}$$

in which $\beta_{H'}$, $\beta_\alpha$, $\beta_J$, and $\beta_\lambda$ are defined as the correction factor $\beta$ influenced by the four aforementioned influence factors, respectively.

The set of conditions $H' = 4$, $\alpha = 0.36$, $J = 80$ kN/m, and $\lambda = 0.15$ were established as a baseline set of conditions, and the correction factor of this condition $\beta'$ is 0.181. The influence of the factor effects was considered to be a type of correction factor. Thus, the following method for determining the value of $\beta$ was defined:

$$\beta = \beta_{H\}} \beta_\alpha \beta_J \beta_\lambda / \beta'^3 \tag{15}$$

Figure 12 shows the influences on $\eta$, which increases with $J$, $H'$, and $\lambda$. There is also a negative correlation between $\alpha$ and $\beta$, except for $\alpha = 0.25$. This is probably because the pile spacing is so large that no soil arching can form in the embankment. This condition is not considered further herein. From the figures mentioned, it has been seen that $\eta$ above the piles changes together with that above the soil. This is because the load above the soil is transferring to the piles via the cushion. The value of $\eta$ above P1 is similar to that above P2 and can be considered to be the same. This is probably because pile caps are the base of arching. Different

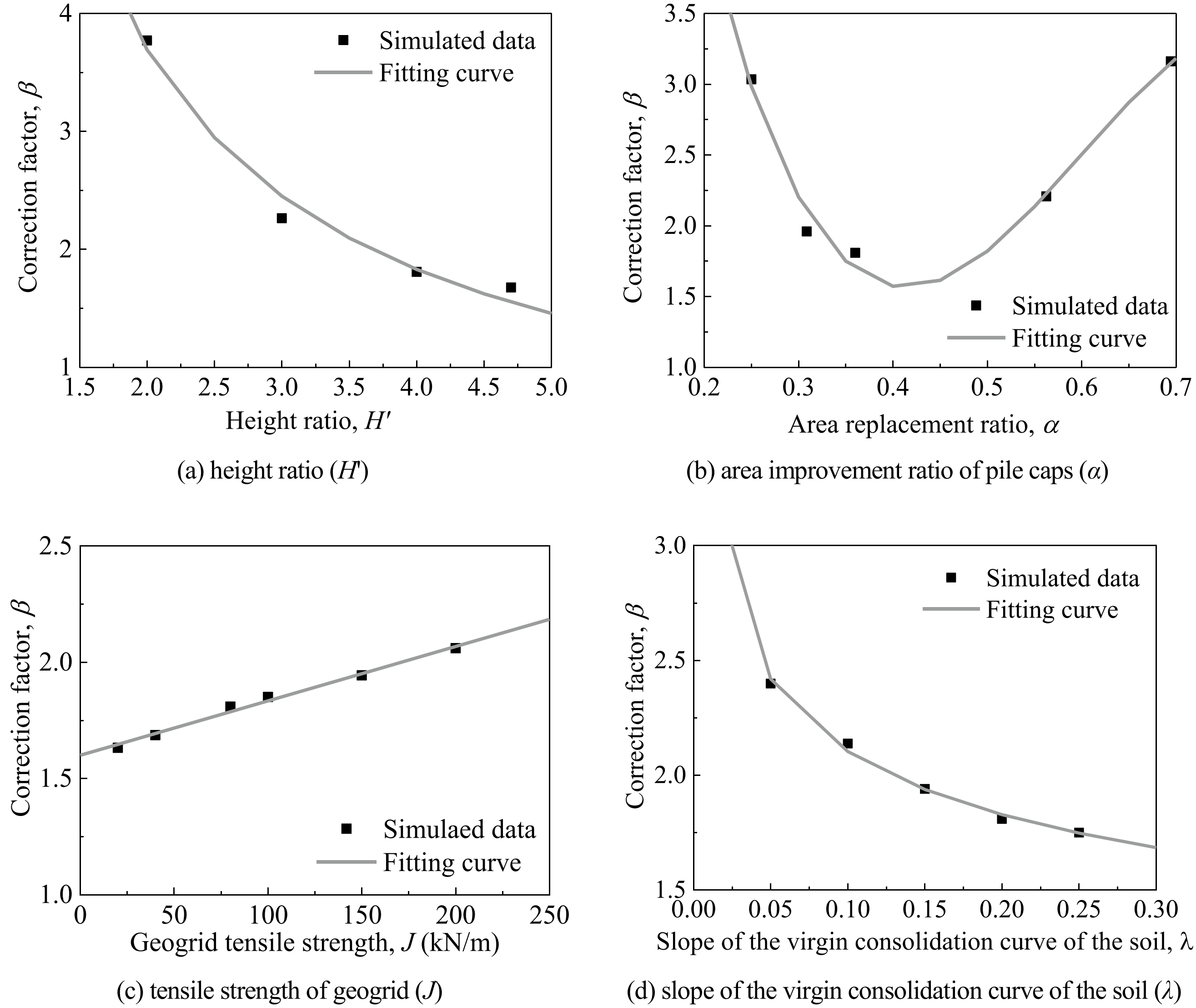


**Fig. 11** Correction factor ($\beta$) influenced by different factors

points on the pile cap correspond with different shells of soil arching, and the stress transfer rates near the base of each soil arching are analogical.

Similar phenomenon can also be seen in the values of $\eta$ above S1 and S2. This is probably because the geogrids embedded in the cushion make cushion a whole, and the stress transfer rates of different points above soil change together in the cushion. The simulated results can be well fitted by the following functions:

$$\eta_{pH'} = 0.722 + 0.225/(1 - 0.816H') \quad R^2 = 0.998 \tag{16}$$

$$\eta_{sH'} = 0.0161H' + 0.255 \quad R^2 = 0.987 \tag{17}$$

$$\eta_{p\alpha} = 0.306 + 0.106/\alpha \quad R^2 = 0.998 \tag{18}$$

$$\eta_{s\alpha} = -0.0326 + 0.13/\alpha \quad R^2 = 0.998 \tag{19}$$

$$\eta_{pJ} = 0.244J^{0.214} \quad R^2 = 0.986 \tag{20}$$

$$\eta_{sJ} = 0.000619J + 0.264 \quad R^2 = 0.990 \tag{21}$$

$$\eta_{p\lambda} = 1.1 + 0.312\ln\lambda \quad R^2 = 0.995 \tag{22}$$

$$\eta_{s\lambda} = 0.571 + 0.158\ln\lambda \quad R^2 = 0.995 \tag{23}$$

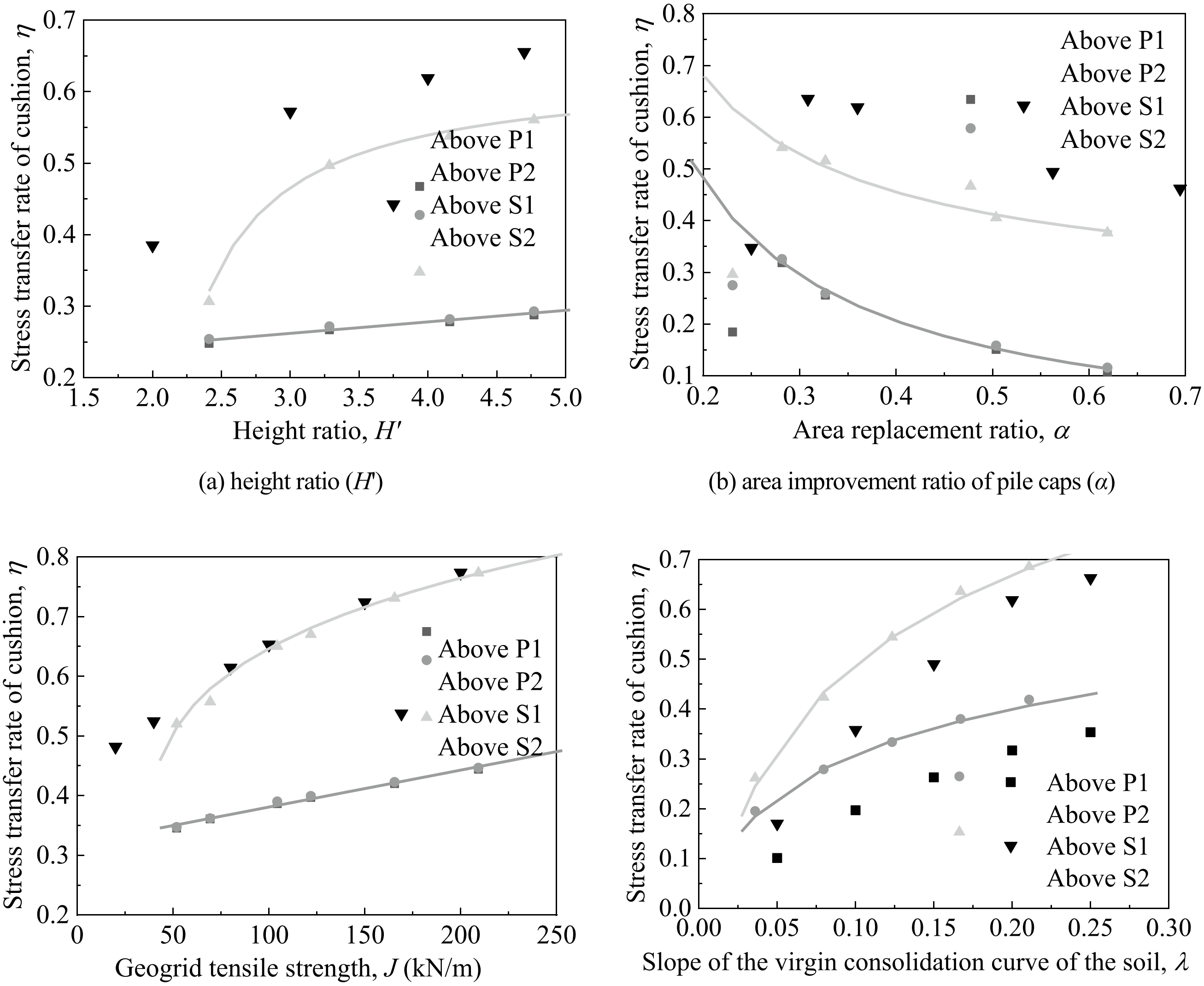


(a) height ratio ($H'$)

(b) area improvement ratio of pile caps ($\alpha$)

(c) tensile strength of geogrid ($J$)

(d) slope of the virgin consolidation curve of the soil ($\lambda$)

**Fig. 12** Stress transfer rate of cushion ($\eta$) influenced by different factors

in which $\eta_p$ and $\eta_s$ are defined as the stress transfer rates of the cushion above the piles and soil, respectively.

The set of conditions $H'=4$, $\alpha=0.36$, $J=80$ kN/m, and $\lambda=0.15$ was established as a baseline. For this condition, stress transfer rate of the cushion $\eta'_p$ is 0.319 and $\eta'_s$ is 0.616. In the same way as $\beta$ is expressed, $\eta_p$ and $\eta_s$ can be expressed as follows:

$$\eta_p = \eta_{pH\}}\eta_{p\alpha}\eta_{pJ}\eta_{p\lambda}/\eta{\prime}_p^3 \tag{24}$$

$$\eta_s = \eta_{sH\}}\eta_{s\alpha}\eta_{sJ}\eta_{s\lambda}/\eta{\prime}_s^3 \tag{25}$$

In a word, in order to calculate the vertical stress above the soil, it is necessary to calculate the stress transfer rate $\eta_s$ using Eqs. (17, 19, 21, 23, 25) and the correction factor $\beta$ using Eqs. (11–15) at first. Then, $\sigma_5$ and $\sigma_6$ can be calculated by Eqs. (1–4). A similar approach applies to the calculation of the vertical stress above the pile.

The simulated pile efficiencies $E_p$ for different conditions and the corresponding fitting curves are shown in Fig. 13.

The simulated $F_p$ can be extracted directly by means of a free body cut in the software. It is apparent that the pile efficiency can be predicted well using the following equations:

$$E_{pH'} = 0.961 - 0.098/(H' - 1.487) \quad R^2 = 0.999 \tag{26}$$

$$E_{p\alpha} = 0.979 - 0.007/(\alpha - 0.223) \quad R^2 = 0.998 \tag{27}$$

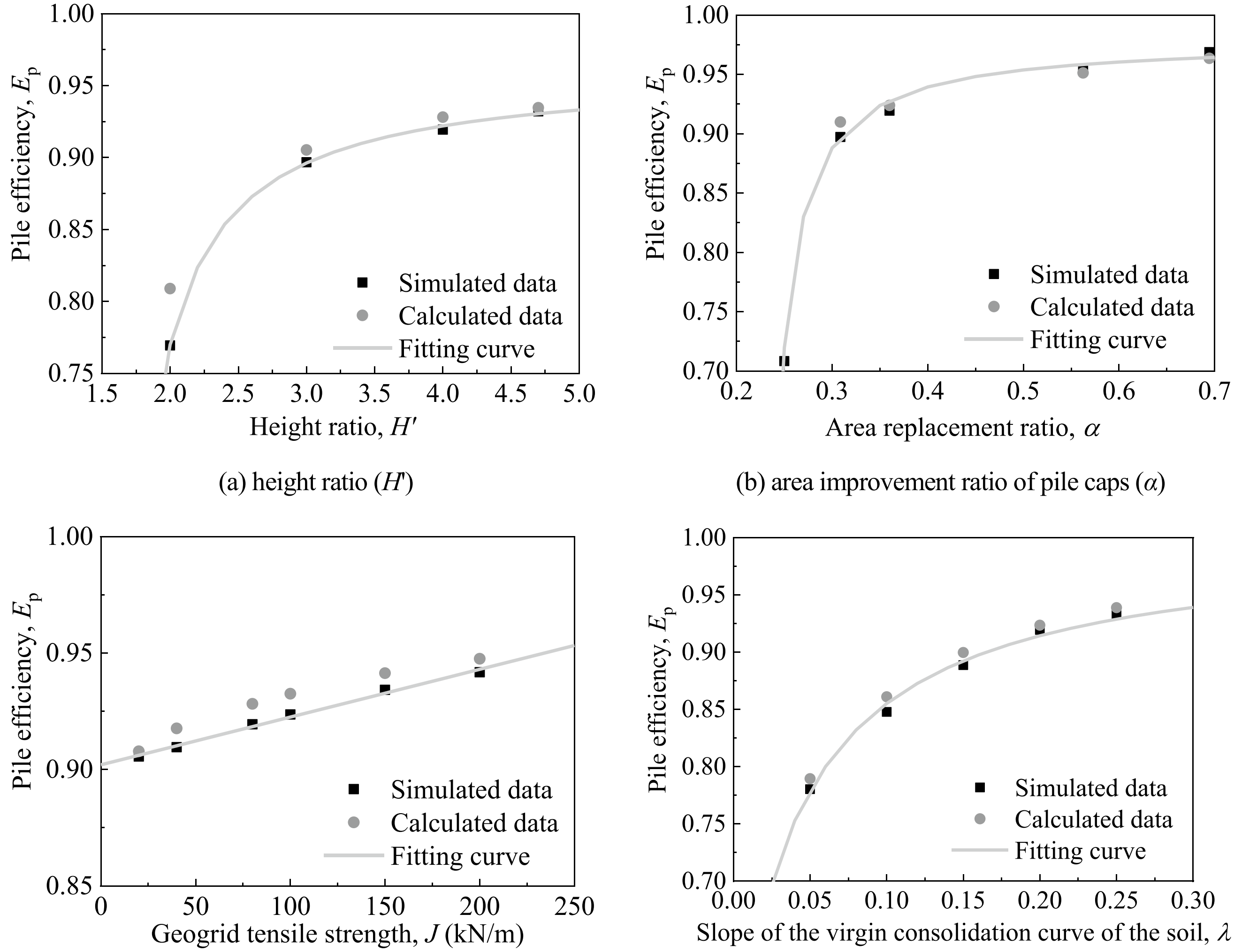


(a) height ratio ($H'$)

(b) area improvement ratio of pile caps ($\alpha$)

(c) tensile strength of geogrid ($J$)

(d) slope of the virgin consolidation curve of the soil ($\lambda$)

**Fig. 13** Pile efficiency ($E_p$) influenced by different factors

$$E_{pJ} = 0.000205J + 0.902 \quad R^2 = 0.997 \tag{28}$$

$$E_{p\lambda} = 1 - 0.021/(\lambda + 0.045) \quad R^2 = 0.993 \tag{29}$$

For the baseline set of conditions, $E'_p$ is 0.919. In the same way as for $\beta$, $E_p$ can be expressed as follows:

$$E_p = E_{pH\}} E_{p\alpha} E_{pJ} E_{p\lambda} / E'^3_p \tag{30}$$

The pile efficiency calculated using the modified empirical model is also shown in the figures. A comparison between the two sets of results reveals no significant differences between the calculated and simulated $E_p$ values. This demonstrates that the modified empirical model can be used effectively to evaluate the vertical stress above the soil on the upper surface of the cushion and evaluate the pile efficiency.

## Conclusions

In this study, field tests and 3-D FEM numerical analyses of the embankment construction process were conducted to investigate the influences of embankment height, pile spacing, tensile strength of the geogrid, and slope of the virgin consolidation curve of the soil on load transfer in GRPSEs. The following conclusions have been drawn from the results obtained.

(1) The numerical model was carefully calibrated to assess the variation in the vertical stress with respect to the measured values. The height ratio of the embankment and the area improvement ratio of the pile caps were found to be the major effects. However, the effects of the tensile strength of geogrid and slope of the virgin

consolidation curve of the soil cannot be neglected. The numerical model was carefully calibrated to assess the variation in the vertical stress with respect to the measured values. The height ratio of the embankment and the area improvement ratio of the pile caps were found to be the major effects. However, the effects of the tensile strength of geogrid and slope of the virgin consolidation curve of the soil cannot be neglected.

(2) The stress transfer rates of different points in the cushion are the same above pile caps and soil, respectively, which can be used to calculate the vertical stress at the upper and lower surfaces of cushion.

(3) The multi-shell arching theory can evaluate the vertical stress at ground level well but not very accurately in the soil arching area. A modified empirical model was developed to calculate the vertical stresses in the embankment, especially in the cushion, and the pile efficiency.

(4) Additional experimental data are needed to further establish a general empirical model, which will be able to consider more influencing factors (e.g. properties of subgrade, temperature, train load, and so on).

**Author Contributions** Conceptualization was performed by MH Yan and SJ Guo; methodology by MH Yan and H Xiao; software by MH Yan and HY Zhang; validation by XG Song and H Xiao; formal analysis by MH Yan and SJ Guo; investigation by MH Yan and XG Song; resources by SJ Guo; data curation by SJ Guo; writing—original draft preparation—by MH Yan; writing—review and editing—by MH Yan; visualization by MH Yan; funding acquisition by MH Yan. All authors have read and agreed to the published version of the manuscript.

**Funding** This work was supported by the Science and Technology Development Project of China Railway Design Corporation under Grant (No. 2022A02538015).

**Declarations**

**Conflict of interest** The authors declare that they have no conflict of interest.

## References

1. Chen JF, Tolooiyan A, Xue JF, Shi ZM (2016) Performance of a geogrid reinforced soil wall on PVD drained multilayer soft soils. Geotext Geomembr 44(3):219–229. https://doi.org/10.1016/j.geotexmem.2015.10.001
2. Ye GB, Cai YS, Zhang Z (2017) Numerical study on load transfer effect of Stiffened Deep Mixed column-supported embankment over soft soil. KSCE J Civ Eng 21:703–714. https://doi.org/10.1007/s12205-016-0637-8
3. Chen RP, Chen YM, Han J, Xu ZZ (2008) A theoretical solution for pile-supported embankments on soft soils under one dimensional compression. Can Geotech J 45(5):611–623. https://doi.org/10.1139/T08-003
4. Liu WZ, Qu S, Zhang H, Nie ZH (2017) An integrated method for analyzing load transfer in geosynthetic-reinforced and pile-supported embankment. KSCE J Civ Eng 21:687–702. https://doi.org/10.1007/s12205-016-0605-3
5. Bhasi A, Rajagopa K (2015) Numerical study of basal reinforced embankments supported on floating/end bearing piles considering pile–soil interaction. Geotext Geomembr 43(6):524–536. https://doi.org/10.1016/j.geotexmem.2015.05.003
6. Zhang CF, Zhao MH, Zhou S, Xu ZY (2019) A Theoretical Solution for Pile-Supported Embankment with a Conical Pile-Head. Appl Sci 9(13):2658. https://doi.org/10.3390/app9132658
7. BS8006–1 (2010) Code of practice for strengthened/reinforced soils and other fills. London, UK: BSI
8. EBGEO (2011) Recommendations for design and analysis of earth structures using geosynthetic reinforcements – EBGEO. German Geotechnical Society, Berlin, Germany
9. Terzaghi K (1943) Theoretical Soil Mechanics. Wiley, New York
10. Guido VA, Kneupel JD, Sweeny MA (1987) Plate load testing on geogrid reinforced earth slabs. In: Proceedings of the Geosynthetics Conference, International Geosynthetics Society, Jupiter, FL
11. Hewlett WJ, Randolph MF (1988) Analysis of piled embankments. In: International journal of rock mechanics and mining sciences and geomechanics abstracts Vol 25 (6), pp 297-298. Elsevier Science
12. Van Eekelen SJM (2015) Basal Reinforced Piled Embankments. Ph.D. Thesis, Delft University of Technology, Delft, the Netherlands
13. Russell D, Pierpoint N (1997) An assessment of design methods for piled embankments. Gro Eng, vol 30(10): pp 9–44. https://trid.trb.org/view/476724
14. Stewart ME, Filz GM (2005) Influence of clay compressibility on geosynthetic loads in bridging layers for column-supported embankments. In: proceedings of the contemporary issues in foundation engineering, geo-frontiers 2005, ASCE, Reston, VA. https://doi.org/10.1061/40777(156)8
15. Naughton PJ, Kempton GT (2005) Comparison of analytical and numerical analysis design methods for piled embankments. In: Proceedings of the Contemporary Issues in Foundation Engineering, Geo-Frontiers 2005, ASCE, Reston, VA. https://doi.org/10.1061/40777(156)11
16. Abdullah CH, Edil TB (2007) Behaviour of geogrid-reinforced load transfer platforms for embankment on rammed aggregate piers. Geosynth Int 14(3):141–153. https://doi.org/10.1680/gein.2007.14.3.141
17. Filz GM, Smith ME (2007) Net Vertical Loads on Geosynthetic Reinforcement in Column-supported Embankments. In: Proceedings of the Geo-Denver 2007, GSP-172: Soil Improvement, Denver, Colorado, United States. https://doi.org/10.1061/40916(235)1
18. Nunez MA, Briançon L, Dias D (2013) Analyses of a pile-supported embankment over soft clay: full-scale experiment, analytical and numerical approaches. Eng Geol 153(8):53–67. https://doi.org/10.1016/j.enggeo.2012.11.006
19. Svanø G, Ilstad T, Eiksund G, Want AA (2000) Alternative calculation principle for design of piled embankments with base reinforcement. In: Proceedings of the 4th International Conference on Ground Improvement Geosystems, Helsinki, Finland. https://www.researchgate.net/publication/327652189_Alternative_calculation_principle_for_design_of_piled_embankments_with_base_reinforcement
20. Chevalier B, Villard P, Combe G (2011) Investigation of load transfer mechanisms in geotechnical earth structures with thin fill platforms reinforced by rigid inclusions. Int J Geomech

11(3):239–250. https://doi.org/10.1061/(ASCE)GM.1943-5622.0000083
21. Zaeske D (2001) Zur Wirkungsweise von unbewehrten und bewehrten mineralischen Trag-schichten ber pfahlartigen Gran dungselementen, Schriftenreihe Geotechnik 10. Kassel University Press GmbH, Kassel, Germany ((**in German**))
22. Wang HL, Chen RP, Liu QW, Kang X (2019) Investigation on geogrid reinforcement and pile efficacy in geosynthetic-reinforced pile-supported track-bed. Geotext Geomembr 47(6):755–766. https://doi.org/10.1016/j.geotexmem.2019.103489
23. Lawson CR (1995) Basal reinforced embankment practice in the United Kingdom. In: Proceedings of the Practice of Soil Reinforcing in Europe, T. S. Ingold, ed., Thomas Telford, London. https://doi.org/10.1680/tposrie.20832.0014
24. Chaimahawan P, Suparp S, Joyklad P, Hussain Q (2021) Finite element analysis of reinforced concrete pile cap using ATENA. Lat Am J Solids Stru 18(2):e342
25. Chango IVL, Assogba GC, Yan MH, Ling XZ, Mitobaba JG (2022) Impact assessment of asphalt concrete in geogrid-reinforced-pile-supported embankment during highspeed train traffic. Balt J Road Bridge E 17(2):135–163
26. Cai DG, Ye YS, Zhang QL, Yan HY, He HW (2009) Field test study on the mechanical behaviors of the geosynthetic-reinforced pile-supported embankment and the deformation of the reinforced bedding. Chi Rai Sci 30(5):1–8
27. Ye GB, Wang M, Zhang Z, Han J, Xu C (2020) Geosynthetic-reinforced pile-supported embankments with caps in a triangular pattern over soft clay. Geotext Geomembr 48(1):52–61. https://doi.org/10.1016/j.geotexmem.2019.103504
28. Huang J, Han J (2010) Two-dimensional parametric study of geosynthetic-reinforcedcolumn-supported embankments by coupled hydraulic and mechanical modeling. Comput Geotech 37(5):638–648. https://doi.org/10.1016/j.compgeo.2010.04.002
29. Adeel MB, Jan MA, Aaqib M, Park D (2021) Development of simulation based p-multipliers for laterally loaded pile groups in granular soil using 3d nonlinear finite element model. Appl Sci 11(1):26. https://doi.org/10.3390/app11010026
30. Bhasi A, Rajagopal K (2013) Study of the effect of pile type for supporting basal reinforced embankments constructed on soft clay soil. Indian J Geosynth Ground Improv 43:344–353. https://doi.org/10.1007/s40098-013-0052-8
31. Leng J, Gabr MA (2005) Numerical analysis of stress-deformation response in reinforced unpaved road sections. Geosynth Int 2(2):111–119. https://doi.org/10.1680/gein.2005.12.2.111
32. Bourgeois E, De Buhan P, Hassen G (2012) Settlement analysis of piled-raft foundations by means of a multiphase model accounting for soil-pile interactions. Comput Geotech 46:26–38. https://doi.org/10.1016/j.compgeo.2012.05.015